# Development of a Lyman-α Detector

T. Kaneyasu[1,2] and M. Kobayashi[3]
[1]*SAGA Light Source, Tosu 841-0005, Japan*
[2]*UVSOR Synchrotron Facility, Institute for Molecular Science, Okazaki 444-8585, Japan*
[3]*National Institute for Fusion Science, Toki 509-5292, Japan*



The attosecond phase-control of electromagnetic radiation from an ultra-relativistic electron is a new capability of synchrotron radiation that allows the control of quantum wave packet interference in the short wavelength regime [1,2]. This unmarked capability of synchrotron radiation has been successfully applied to quantum control and ultrafast spectroscopy of atoms in the extreme ultraviolet wavelength. As a next step of the quantum control by synchrotron radiation, we plan to observe the quantum interference between the vibrational wave packets in the hydrogen molecule excited by vacuum ultraviolet (VUV) pulses.

In the designed experiment, the hydrogen molecule interacts with a pair of VUV pulses. The quantum interference between the vibrational wave packets is monitored by detecting the fluorescence in the ultraviolet wavelength. In particular, the Lyman-α emission from a fragment can be used to probe the vibrational excitation in a particular state [3].

Figure 1 shows the developed detector. The Lyman-α detector consists of a gas cell and a micro-channel plate (MCP). The gas cell is equipped with a $MgF_2$ window which allows selective detection of fluorescence larger than 120 nm wavelength. The MCP is coated with CsI to increase the quantum efficiency in the VUV wavelength.

As a performance test of the detector system, we have measured the fluorescence yield spectrum of hydrogen molecules in the VUV wavelength at BL7B. The detection angle was set to be 55 degrees with respect to the polarization vector of the synchrotron radiation. A Nb filter of 160 nm thickness was inserted in front of the experimental chamber to filter out the second harmonic and to maintain the ultrahigh vacuum condition in the beamline.

Figure 2 shows the fluorescence yield spectrum where we have assigned three vibrational progressions belonging to the B $^1\Sigma_u^+$, C $^1\Pi_u$, and D $^1\Pi_u$ electronic states according to the EELS study [4]. The Lyman-α from the D state is attributed to the production of H(2*l*) atoms generated by the predissociation of the vibrationally excited states. In contrast to the spectrum measured with a detector equipped with a ceratron [3], the fluorescence yield from the B and C states is enhanced in the observed spectrum. They are most likely a consequence of the molecular fluorescence of more than 150 nm wavelength emitted from these states [5]. Given that the relative quantum efficiency of the CsI-coated MCP for the 150 nm wavelength is about one order of magnitude higher than that for the Lyman-α wavelength [6], the fluorescence intensity is enhanced in the region of the B and C states. The performance of the detector is satisfactory, and its application to the quantum interference experiment is planned.

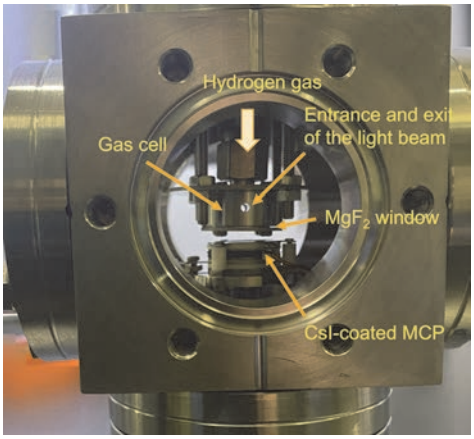


Fig. 1. Photo of the Lyman-α detector. The detector components were assembled inside the ICF-70 cube-type chamber.

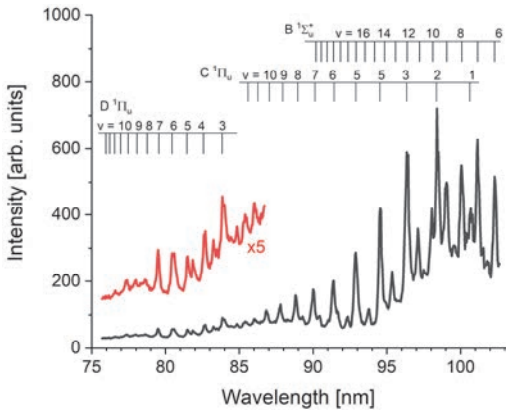


Fig. 2. VUV fluorescence yield spectrum measured by the Lyman-α detector.

[1] Y. Hikosaka *et al.*, Nat. Commun. **10** (2019) 4988.
[2] T. Kaneyasu *et al.*, Phys. Rev. Lett. **126** (2021) 113202.
[3] S. Arai *et al.*, Z. Phys. D **4** (1986) 65.
[4] W. F. Chan *et al.*, Chem. Phys. **168** (1992) 375.
[5] P. Schmidt *et al.*, J. Phys. Conf. Ser. **635** (2015) 112130.
[6] Kuwabara *et al.*, JAXA-RR-16-011 (2017).

BL7B

# Evaluation of Fluorescence Lifetimes of UV-Cured Scintillators for the Next $K_L^0$ Rare Decay Experiment at J-PARC

Y. Tajima[1], R. Abe[1], T. Naito[1], Y. Honma[1], N. Izawa[1], S. Yamamoto[1] and H. Y. Yoshida[1]
[1]*Department of Science, Yamagata University, Yamagata 990-8560, Japan*

J-PARC E14 KOTO [1] is the current running experiment of searching for the direct CP violating decay $K_L \to \pi^0\nu\bar{\nu}$ decay. This decay mode is considered to be sensitive to new physics beyond the Standard Model (SM), and its branching ratio is predicted to be $3.0 \times 10^{-11}$ in the SM with about 2% theoretical uncertainly. The upper limit currently obtained on the branching fraction of $K_L \to \pi^0\nu\bar{\nu}$ decay is $2.2 \times 10^{-9}$ at the 90% confidence level [2].

We are planning the next generation $K_L \to \pi^0\nu\bar{\nu}$ experiment, called KOTO-II [3]. KOTO-II experiment uses a beam intensity about three times higher and a decay volume about five times longer than that of KOTO. The operation of the detectors in KOTO-II are required higher counting rates. To satisfy this requirement, the scintillators need to have a short fluorescence lifetime, which enables fast time response.

Recently, a new UV-cured scintillator with high light yield has been developed [4]. The scintillators are expected to be easy to fabricate and low cost.

We are currently evaluating its various characteristics for use in KOTO-II experiment. For this purpose, the fluorescence spectrum and decay curve of a newly developed high light yield UV-cured plastic scintillator were measured in this experiment.

The fluorescence decay curves were measured by using light pulses from visible to near ultraviolet under single bunch operation, which enables a time-correlated single-photon counting.

In this experiment, ethoxylated bisphenol A diacrylate (EBECRYL 150 supplied from Daicel Allnex) was used as the host polymer, Irgacure TPO as the photoinitiator, DPO and POPOP as wavelength shifters.

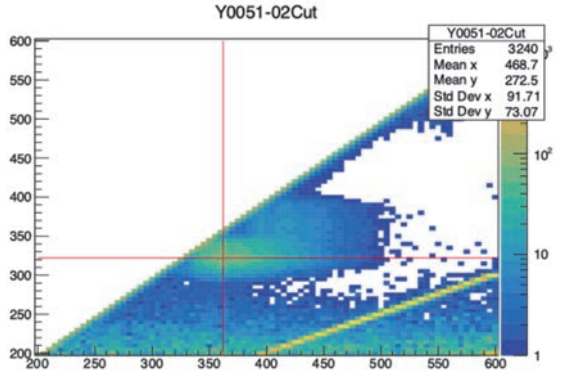


Fig. 1. 2D fluorescence spectra of the UV-cured host polymer. Y-axis is excitation wave length (nm) and X-axis is emission wave length (nm).

Figure 1 shows the 2D fluorescence spectra of the UV-cured host polymers and Fig. 2 shows of the UV-cured scintillator. Figure 3 shows the decay curves. The blue line is the data of the host polymer for the 392 nm band under excitation at 240 nm, the red line is the data of the scintillator data for the 450 nm band under excitation at 322 nm.

Now that we have established a basic evaluation method for UV-cured scintillators, we plan to evaluate other UV-cured scintillators.

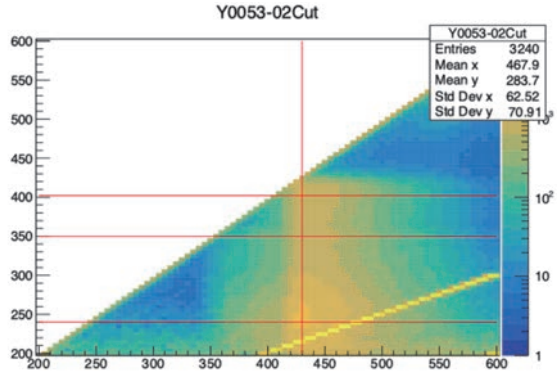


Fig. 2. 2D fluorescence spectra of the UV-cured host polymer with DPO and POPOP.

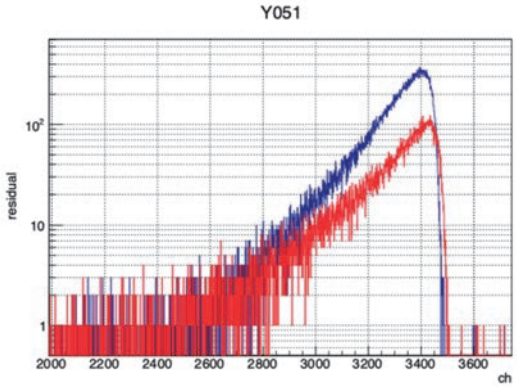


Fig. 3. Decay curve of the UV-cured host polymer (blue) and UV-cured scintillator (red). (946ch/ns)

[1] J. Comfort *et al.*, Proposal for $K_L \to \pi^0\nu\bar{\nu}$ Experiment at J-PARC (2006).
[2] J.K. Ahn *et.al.*, Phys. Rev. Lett. **134** (2025) 081802.
[3] J.K. Ahn *et.al.*, J-PARC PAC (arXiv 2501.14827).
[4] N. Hayashi and M.Koshimizu, J. Lumin. **277** (2025) 120993.

BL7B

# Excitation Spectra of Plastic Scintillators Based on PVK Containing Different Organic Fluorescent Molecules

M. Koshimizu[1]

[1]*Research Institute of Electronics, Shizuoka University, 3-5-1 Johoku, Chuo-ku, Hamamatsu 432-8011, Japan*

Scintillators are a kind of phosphors that can be used for radiation detection in combination with photon detectors (e.g. photomultiplier tubes) to form scintillation detectors, where scintillation photons upon impinge of ionizing radiation are converted and amplified into electric pulsed signals. Because the response speed of the photon detectors is faster than the decay of the scintillation of scintillators in most cases, scintillators exhibiting fast scintillation decay is necessary to achieve excellent timing resolutions or detection capability at high counting rate with short dead time. From the viewpoint of fast response, plastic scintillators are favorable owing to their fast scintillation decay with typically < 10 ns, which is much faster than those of inorganic scintillators [1, 2]. In addition, scalability and low production cost of the plastic scintillators are favorable to large-scale detectors used in high-energy and particle physics. A significant drawback of the plastic scintillators is low scintillation light yield of typically ~10,000 photons/MeV or less, which is significantly smaller than those of inorganic scintillators. A cause of this low scintillation yield is the formation of triplet excited states in the host polymer, which is formed upon recombination of electron–cation pairs after ionization. The use of the triplet states is the key to enhance the scintillation light yield of plastic scintillators.

Recently, triplet excited states have been efficiently used for photon emission in organic light-emitting diodes via efficient phosphorescence or thermally activated delayed fluorescence. If such utilization of triplet excited states is possible in plastic scintillators, one can enhance scintillation light yield in plastic scintillators. To achieve the scintillation light yield in this approach, it is necessary to develop appropriate fluorescent molecules that can convert the energy of triplet excited states into photons via delayed fluorescence or phosphorescence and a technique to analyze the contribution of photon emission originated from triplet excited states. Recently, we found that the contribution of emission originating from singlet and triplet excited states can be analyzed based on excitation spectra in VUV region [3] and difference in the decay behavior at different excitation wavelengths in VUV—UV region [4]. In the previous study, we have analyzed the properties of plastic scintillators based on polystyrene. In this study, the emission properties of plastic scintillators based on polyvinyl carbazole (PVK) were analyzed.

The samples were plastic scintillators based on PVK containing POPOP, bis-MSB, TPB, or DPA as the fluorescent molecules. The photoluminescence spectra of the samples under VUV irradiation at different wavelengths were obtained at BL7B of UVSOR, Institute for Molecular Science, Japan. Based on the photoluminescence spectra and the excitation light intensity as functions of excitation wavelength, we obtained excitation spectra in VUV region.

Excitation spectra of the samples containing bis-MSB and DPA are presented in Figs. 1 and 2, respectively. The spectra were similar regardless of the contained organic fluorescent molecules. The spectra were also similar to those of polystyrene-based plastic scintillators [3].

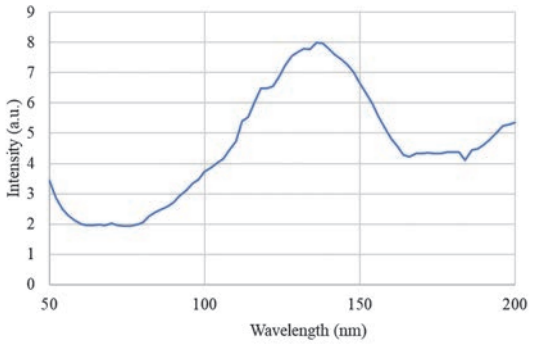


Fig. 1. Excitation spectra of PVK-based plastic scintillators containing bis-MSB.

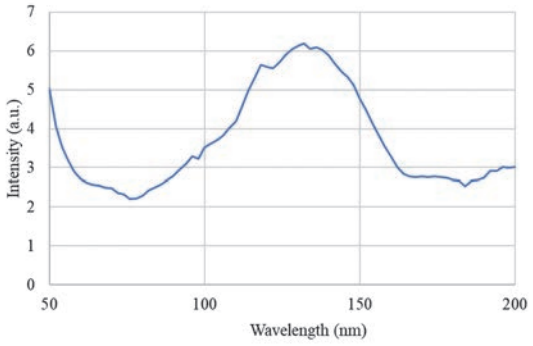


Fig. 2. Excitation spectra of PVK-based plastic scintillators containing DPA.

[1] M. Koshimizu, Jpn. J. Appl. Phys. **62** (2023) 010503.
[2] M. Koshimizu, J. Lumin. **278** (2025) 121008.
[3] M. Koshimizu, Y. Fujimoto, and K. Asai, UVSOR Activity Report **50** (2022) 111.
[4] M. Koshimizu, UVSOR Activity Report **51** (2023) 118.

BL7B

# Vacuum Ultraviolet Characterization of Li-Glass as a Potential Neutron Scintillator

T. Shimizu[1], K. Shinohara[1], K. Yamanoi[1] and N. Sarukura[1]
[1]*Institute of Laser Engineering, The University of Osaka, 2-6 Yamadaoka Suita, Osaka 565-0875 Japan*

In nuclear fusion experiments, neutron detection plays a vital role in monitoring both operational efficiency and radiation safety. Primary neutrons, being high in flux, are typically detected using conventional plastic scintillators. However, scattered neutrons, generated through secondary nuclear reactions and arriving with a time delay, are present in much smaller quantities. Their reliable detection demands scintillators with high neutron sensitivity and fast optical response to distinguish their signals from primary neutrons and associated X-rays.

Scattered neutrons generally possess energies in the range of 0.2 to 0.6 MeV. $^{6}$Li is known to have a high neutron absorption cross-section within this energy range, and $^{6}$Li-containing glass scintillators doped with $Ce^{3+}$ have long been employed for thermal neutron detection. Commercial products such as GS2, GS20, and KS20 are based on $Ce^{3+}$-doped $Li_2O$–$SiO_2$ glass matrices. However, these materials exhibit luminescence decay times of 50–70 ns, insufficient for the 25 ns time resolution required in time-of-flight (TOF) neutron measurements.

To address this issue, a new type of scintillator based on a $20Al(PO_3)_3$–80LiF (APLF) glass matrix was developed. This material offers superior UV transparency and minimal self-absorption, making it ideal for shorter-wavelength luminescence. By replacing $Ce^{3+}$ with $Pr^{3+}$, the emission wavelength was shifted from 300–350 nm to 250–300 nm, effectively shortening the luminescence decay time.

Previously, We have compiled the analysis and discussion of the X-ray absorption near edge structure (XANES) spectroscopy for the presence of Pr ions in the glasses with a oxidation state.[1] .

In addition to APLF, we investigated alternative lithium glass matrices for scintillator use. Collaborative efforts led to the development and evaluation of various Pr-doped lithium glasses: $20Li_2O$–$20CaO$–$60SiO_2$+ $0.3Pr_2O_3$(LCSO+0.3Pr), $30Li_2O$–$70B_2O_3$+$0.3Pr_2O_3$ (LBO+ 0.3Pr), $30Li_2O$–$60P_2O_5$–$10Al_2O_3$ + $0.3Pr_2O_3$ (LPA+ 0.3Pr).[2]

In FY2024, we will focus on LPA-type glasses with varied Pr concentrations, as they have shown promise in luminescence control. The samples under evaluation include: LPA10+0.1Pr, LPA10+0.3Pr, LPA10+0.5Pr, LPA10+1Pr, LPA10+2Pr. All samples are solid, non-volatile, and pose no safety concerns.

Spectral measurements were conducted at the UVSOR synchrotron facility using the VUV beamline. A combination of spectrometers, cooled CCD cameras, and photomultiplier tubes (PMTs) was used to measure transmission, absorption, and emission spectra. The samples were placed in a vacuum chamber (pressure < $1.0 \times 10^{-5}$ Pa) and irradiated with 100–180 nm synchrotron radiation. Si photodiodes were used for transmission measurements, while luminescence was detected using PMTs and CCD cameras. Temperature-controlled experiments were performed from liquid helium temperature up to room temperature, and emission was recorded in the 200–800 nm range. The excitation wavelengths were selected based on prior photoluminescence excitation spectra.

The transmission spectra for the LPA samples showed a systematic shift in the absorption edge corresponding to varying Pr concentrations, indicating successful doping (Fig.1). However, attempts to measure luminescence spectra were hindered by reduced system sensitivity. The resulting emission signals were too weak for reliable detection under the current measurement setup.

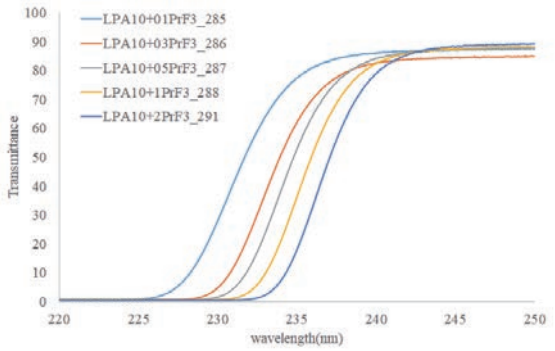


Fig. 1. Transmission spectrum for the LPA.

Although the absorption behavior of the Pr-doped LPA glasses was clearly characterized, luminescence measurements remain inconclusive due to instrumentation limitations. Future experiments will focus on improving measurement conditions and signal screening methods to enable effective evaluation of emission and excitation spectra. Once optimized, these measurements will guide the assessment of scintillator performance and help identify the most suitable material composition for scattered neutron detection.

[1] K. Shinohara *et al.*, the 9th International Symposium on Optical Materials (IS-OM'9), Tarragona (Spain), from June 26 to 30, 2023.
[2] T. Shimizu *et al.*, UVSOR Activity Report **51** (2023) 119.

# Optical Properties of Rare-Earth Doped $La(BO_2)_3$ Phosphor for Radiation Detection

J.Y. Cho[1], E.J. Choi[1], D.W. Jeong[1], N.D. Ton[1] and H.J. Kim[1]
[1]*Department of Physics, Kyungpook National University, Daegu 41566, Republic of Korea*



Borate-based materials are of considerable interest due to their optical transparency, wide bandgap, and thermal and chemical stability, making them ideal hosts for rare-earth dopants in luminescent applications. In particular, lanthanum borates such as $La(BO_2)_3$ offer a stable crystal environment that supports efficient energy transfer and emission. When doped with rare-earth ions like $Nd^{3+}$, $Eu^{3+}$, and $Pr^{3+}$, these materials exhibit promising luminescence properties suitable for lasers, phototherapy, and radiation detection [1–3].

However, studies on $La(BO_2)_3$ phosphors doped with $Ce^{3+}$ and $Tb^{3+}$ remain limited. This work focuses on investigating the luminescence behavior of Ce, Tb co-doped $La(BO_2)_3$ using PL, PLE, and VUV excitation (BL7B beamline), aiming to elucidate their emission mechanisms and assess their potential for optical applications.

In addition, since $La(BO_2)_3$ can be fabricated both as glass and as a crystalline phosphor, we aim to investigate the differences in their luminescence properties through VUV spectroscopy.

The samples were prepared via solid-state reaction at 900 ˚C for 10 hours from $La_2O_3$ and $H_3BO_3$ powder as starting materials and $CeBr_3/Tb_4O_7$ activator. After the mixing process,the mixtures were loaded in alumina crucibles and placed in a high-temperature round furnace where the solid-state reactions occurred. Finally, the products were ground in an agate mortar then introduced to XRD measurement to confirm the crystallization structures before pelletized with a hydraulic press.

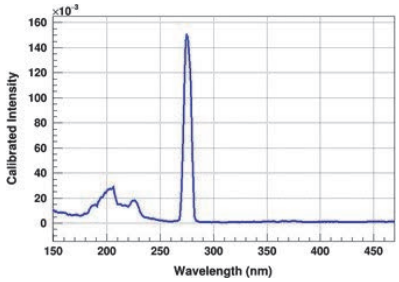


Fig. 1. Calibrated excitation spectrum of $La(BO_2)_3$:Tb phosphor.

Under the excitation measurement of 545 nm emission on $La(BO_2)_3$:Tb phosphor, broad bands from 180-240 and an intense peak of 270-285 nm were observed as shown in Fig.1. The broad band at 180-240 nm could be explained by the transitions from low energy levels to 4f levels of $Tb^{3+}$ while the prominent peak appears at 270–280 nm, indicating the most efficient excitation wavelength for terbium ($Tb^{3+}$) emissions at 545 nm is characteristic of 4f → 5d transitions for $Tb^{3+}$. The PL excitation spectrum of $La(BO_2)_3$:Tb confirms that the material can be efficiently excited at 270–285 nm to produce the 545 nm emission then making it the potential choice for applications like phosphors in lighting or display technologies where $Tb^{3+}$'s green emission is desired.

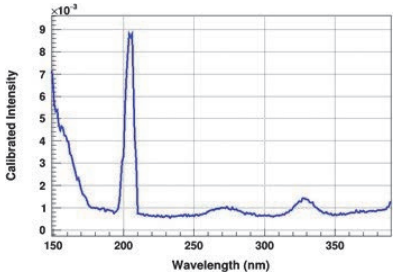


Fig. 2. Calibrated excitation spectrum of $La(BO_2)_3$:Ce phosphor.

Meanwhile, the excitation spectrum of $La(BO_2)_3$: Ce corresponding to 400 nm emission as shown in Fig. 2 is primarily dominated by a strong transition near 200 nm, making it effective for deep-UV-excited blue emission applications. Besides, weak bands from 260 - 290 nm and 320-350 nm were observed. The weak response at higher wavelengths limits its efficiency under near-UV excitation sources but could still contribute to broad-spectrum phosphor applications.

[1] X. Wang *et al*., Mater. Res. Bull. **52** (2014) 112.
[2] J. Guohua *et al*., Crystal Opt. Commun. **242** (2004) 79.
[3] T. Dogan *et al*., Ceram. Int. **45** (2019) 4918.

BL7B

# High-Resolution Photoelectron Spectroscopy of Functional Compounds with High Melting Points

H. Kohguchi[1], Y. Hikosaka[2], T Kaneyasu[3], S. Wada[1], K. Shimizu[4], M. Katoh[1,4] and Y-I. Suzuki[5]

[1]*Graduate School of Advanced Science and Engineering, Hiroshima University, Higashi-Hiroshima 739-8526, Japan*

[2]*Institute of Liberal Arts and Sciences, University of Toyama, Toyama 930-0194, Japan*

[3]*SAGA Light Source, Tosu 841-0005, Japan*

[4]*UVSOR Synchrotron Facility, Institute for Molecular Science, Okazaki 444-8585, Japan*

[5]*School of Medical Technology, Health Sciences University of Hokkaido, Tobetsu 061-0293, Japan*

Photoelectron circular dichroism (PECD) has been investigated with a photoelectron imaging apparatus based on the velocity-mapping imaging (VMI) methodology. The targets of the PECD study have been mostly limited to gaseous or volatile samples since photoelectron imaging relies on electron detection under high vacuum conditions. Chiral compounds in solid form are not subjects of the PECD study, although much more chiral species with novel chirality are stable than gaseous and volatile liquid samples. We have developed the VMI photoelectron imaging apparatus for PECD measurement, providing high-quality PECD data for gaseous chiral molecules [1]. Application of the VMI apparatus to solid chiral samples requires the generation of the molecular beam by heating solid samples. The molecular beam intensity was found to be much weaker than that of the gaseous beams in our previous studies [2]. Thus, efficient photoelectron data collection is a key to PECD measurements of solid chiral species as well as intense beam sources with a heat nozzle.

A photoelectron count rate for gaseous samples is typically several hundred kcps under our experimental conditions. Although the count rate can be increased by more than 1000 kcps, our previous image detection system could only acquire less than 100 kcps photoelectrons because of the slow frame transfer rate (33 frames/s) of the camera system. In the present measurement with the BL7B beamline, we have adopted an event-driven camera to a spot image of a photoelectron arrival on the phosphor screen, whose nominal response time is potentially one microsecond.

We examined the sensitivity and operative limitation of the event-driven camera for the actual PECD measurement conditions but the Ar sample was used for evaluation. The results of photoelectron imaging of Ar at 76 nm photoionization are shown in Fig. 1. The photoelectron image obtained with the conventional frame camera exhibited noticeable background noise outside of photoelectron scattering distribution (Fig. 1a). The background, which originated from the analog recording, was found to be critical for in our previous PECD study because difference image data between right- and left circularly polarization ionization is heavily affected by preceding signal normalization. It is noted that the electron background, which originates from the photoionization of the imperfectly evacuated samples in the vacuum chamber subtraction, is not problematic in image subtraction. The image data captured with the event-driven camera at various count rates (Fig. 1b-1d) indicated that no photoelectron arrival position on the phosphor screen was lost up to the count rate of 180 kcps. The photoelectron spectra and the angular distributions with 5 kcps, 40 kcps, and 180 kcps are identical other than the signal statistics. Application of the event-driven camera to the photoelectron imaging with synchrotron radiation, especially to the image subtraction, is thus confirmed.

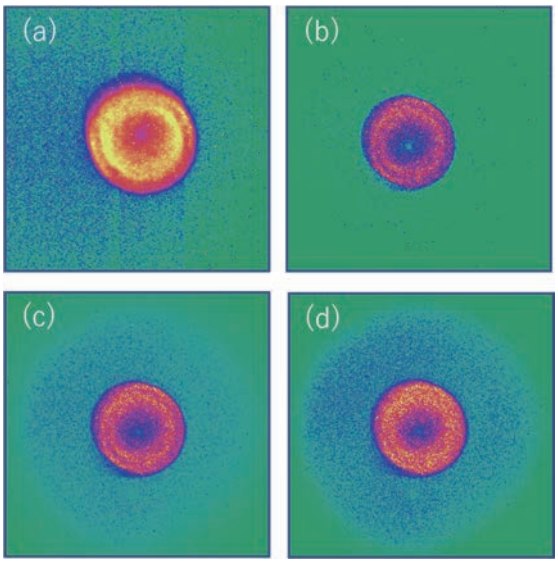


Fig. 1. Photoelectron scattering images of Ar at 76 nm photoionization with (a) the frame-camera (conventional) and (b)–(d) the event-driven camera. The electron count rate is (b) 5 kcps, (c) 40 kcps and (d) 180 kcps. The outside of the double-ring image is especially emphasized to display the background level.

[1] H. Kohguchi *et al.*, UVSOR Activity Report **50** (2023) 138.

III-3

BL7B

# Polarization Dependence of Solid-Liquid Interfaces Probed by Attenuated Total Reflectance Ultraviolet (ATR-UV) Spectroscopy

I. Tanabe[1], T. Kakinoki[2] and K. Fukui[2]
[1]*Department of Chemistry, College of Science, Rikkyo University, Toshima 171-0021, Japan*
[2]*Department of Materials Engineering Science, Graduate School of Engineering Science, The University of Osaka, Toyonaka 560-8531, Japan*

Electric double-layer organic field-effect transistors (EDL-OFETs) have garnered significant interest for their ultra-low operating voltage (<1 V), which is markedly lower than that of conventional $SiO_2$-gated OFETs (>10 V). This reduced voltage is achieved through the formation of a high electric field within the electric double layer (EDL), which accumulates at the interface between the organic semiconductor and the electrolyte. Consequently, understanding and optimizing the organic semiconductor/electrolyte interface is crucial for the performance of EDL-OFETs.

Attenuated Total Reflection (ATR) spectroscopy is a useful method for studying interfaces. In particular, in the ultraviolet (UV) region, it provides valuable information about the electronic states of materials. We have previously utilized ATR-UV spectroscopy with a deuterium lamp as a light source to investigate the interfaces between organic semiconductors or metals and electrolytes [1, 2]. Through this approach, we have elucidated the electronic states of organic semiconductors and interfacial electrolytes depending on the applied voltage. While a deuterium lamp emits unpolarized light, the use of polarized light is expected to provide insights into the orientation of organic semiconductors and interfacial electrolytes. Therefore, in this study, we aimed to develop a new spectroscopic system utilizing polarized light obtained from BL7B at UVSOR.

A thin film of C9-DNBDT-NW (Figure 1a), a material reported to exhibit excellent mobility, was deposited onto a sapphire ATR prism and measured using ATR setup. By adjusting the orientation of the prism relative to the incident light, the polarization characteristics of the spectra were investigated. The results, shown in Figures 1b and 1c, reveal a clear polarization dependence. As shown in Figure 1b, *s*-polarized incident light produced distinct absorption peaks within the 200–500 nm range, whereas *p*-polarized light exhibited no such prominent features(Figure 1c).

Figures 1d and 1e illustrate the polarization-dependent absorption spectra of C9-DNBDT-NW, as calculated using time-dependent density functional theory (TD-DFT). The results indicate that along the x-axis (Figure 1d), multiple strong absorption features were predicted, whereas along the z-axis, almost no absorption was observed. Considering the experimental results, it is suggested that this thin film is structured with the x-axis oriented perpendicularly to the substrate.

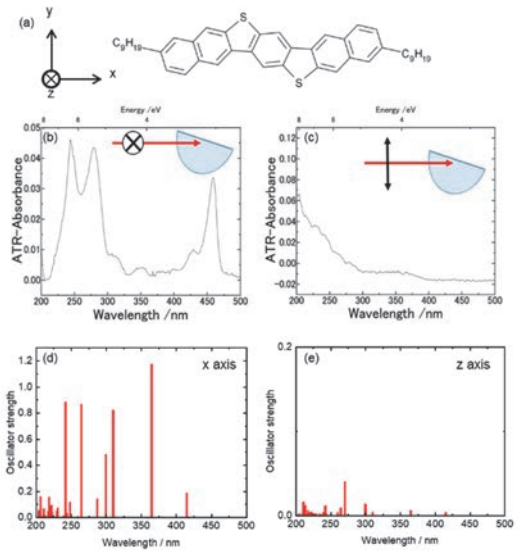


Fig. 1. (a) The structural formula of C9-DNBDT-NW. (b, c) Polarization dependence of ATR spectra of C9-DNBDT-NW on a sapphire prism. (d, e) Calculated vertical transitions along (d) x- and (e) z-axis of a C9-DNBDT-NW molecule.

Thus, polarization-dependent ATR spectroscopy enables the determination of the molecular orientation in organic thin films deposited on a sapphire substrate. Additionally, a key feature of ATR spectroscopy in the ultraviolet region is its short probing depth, limited to tens of nanometers due to the penetration depth of the evanescent wave. Moreover, by adjusting the incident angle, this probing depth can be finely controlled on the nanometer scale. Further advancements in this technique are expected to enable the investigation of electrochemical responses and the organic semiconductor-electrolyte interface.

[1] I. Tanabe *et al.*, Anal. Chem. **91** (2019) 3436.
[2] I. Tanabe *et al.*, Commun. Chem. **4** (2021) 88.

BL7B

# Investigation of Space Weathering Effects on PAHs Using Laboratory Simulations

C. Wu[1], S. Liu[1], K. Yoshioka[1] and I. Yoshikawa[1]
[1]*Department of Complexity Science and Engineering, Graduate School of Frontier Sciences, The University of Tokyo, Chiba 277-8561, Japan*

Polycyclic aromatic hydrocarbons (PAHs) are widespread cosmic organic molecules. The PAH hypothesis indicates a 217.5 nm absorption bump of the interstellar extinction curve may be attributed to the PAH molecule. This theoretical hypothesis was supported by an experiment of Joblin et al. [1] Additionally, space weathering refers to the physical and chemical changes that occur on the surfaces of airless bodies or objects when exposed to interplanetary environments, resulting in alterations to their spectroscopic features. One significant effect should be noted, this process may cause absorption bands to shift towards longer wavelengths after exposure. There are various approaches to studying space weathering, including the early analysis of Apollo samples and subsequent irradiation experiments conducted on the International Space Station. Among these methods, laboratory simulations of space weathering have become a widely used research technique.

In this study, we employed UV irradiation experiments using 0th-order light on coronene. Subsequently, we utilized beamline BL7B to measure the transmittance spectra of the samples exposed to 0th-order light and unexposed.

In the irradiation experiments, coronene samples were subjected to irradiation for durations of 3 hours, 6 hours and 8 hours, utilizing the 0th-order light from BL7B.

In the transmittance spectra measurement experiment, a photodiode was utilized. The detailed experiment structure can be seen in Fig.1. Additionally, for reducing the effect of higher-order light to obtain more accurate results, various gratings and filters combinations were utilized. Specifically, the setups included the G2 grating plus Quartz and Pyrex filters, as well as G3 grating plus Quartz and Pyrex filters.

In calculating absorption spectrum, due to samples and substrates being too thin, which causes the reflectance to be negligible compared to the transmittance. Therefore, the absorption ratio can be calculated by 100% minus the transmittance ratio. Consequently, the absorption spectrum in Fig.2 can be obtained.

According to the results on Fig. 2, the absorption spectrum has altered after 3-hour and 8-hour of 0th-order light irradiation, compared to the spectrum without irradiation. The detailed performance is peak shift towards shorter wavelengths. The reason for peak shift was considered the hydrogen atom loss.

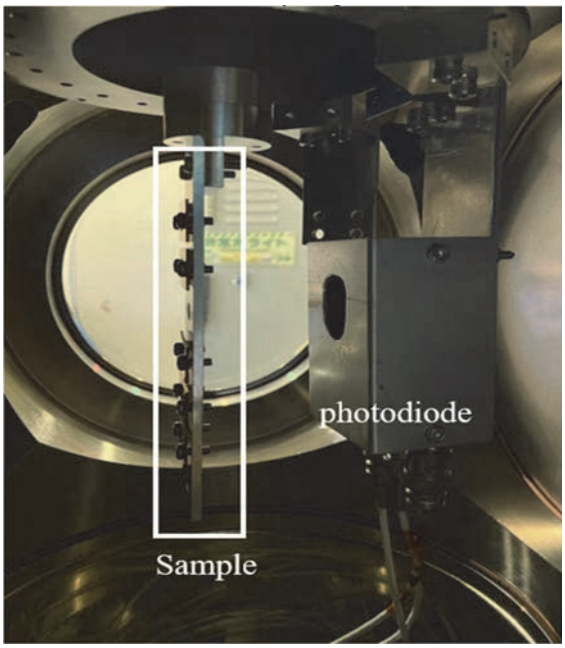


Fig. 1. Spectra measurement experiment.

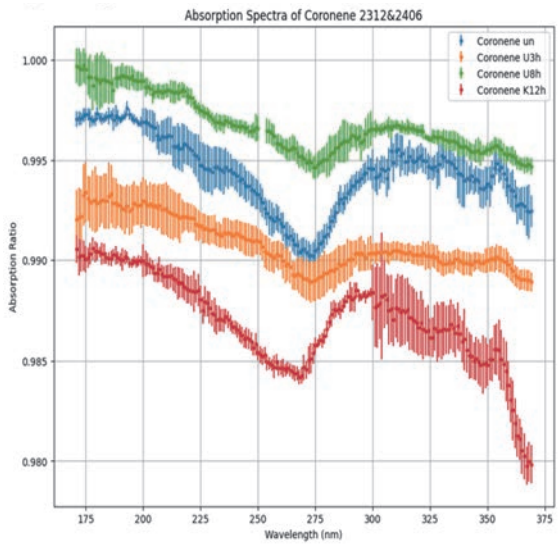


Fig. 2. Absorption spectra of coronene exposed and unexposed.

[1] C. Joblin *et al*., Astrophys. J. **393** (1992) L79.

III-5